ELSEVIER

Journal of Molecular Structure (Theochem) 395–396 (1997) 29–40

THEO CHEM

The conformational space of selected aldo-pyrano-hexoses

Gábor I. Csonka[a,*], István Kolossváry[b], Pál Császár[c], Krisztina Éliás[a], Imre G. Csizmadia[c]

[a]*Department of Inorganic Chemistry, Technical University of Budapest, H-1521 Budapest, Hungary*
[b]*Department of Chemical Information Technology, Technical University of Budapest, H-1521 Budapest, Hungary*
[c]*Department of Chemistry, University of Toronto, Toronto, Ont. M5S 1A1, Canada*

Received 11 December 1995; accepted 20 February 1996

Abstract

The conformational space of selected aldo-pyrano-hexoses was searched by the MM2*–SUMM (systematic unbounded multiple minimum) molecular mechanics conformational search technique. The first 19 structures of lowest energy were analyzed at the HF/3-21G, 6-31G(d) and generalized gradient approximation–density functional (GGA–DFT) levels of theory. The interactions of the hydroxyl groups were analyzed by employing the gradient vector field theory. © 1997 Elsevier Science B.V.

Keywords: Energy; D-Glucose; D-Mannose; MM2*; Hartree-Fock; Density Functional Theory; Structure

1. Introduction

In aqueous solutions the 16 D-aldo-hexoses exist almost exclusively in the pyranosyl (6-membered ring) form. These rings take either of two non-equivalent chair forms [1] or, in a few instances, also populate skew or skew-boat forms [2]. For any given ring form, the, three-fold rotations of the four hydroxyl and the hydroxymethyl groups can generate $3^6 = 729$ different rotamers. Not all of these will be stable. However, it is expected that there will be numerous fairly stable forms for each sugar.

The conformers of four aldo- hexoses (α- and β-D-glucose and α- and β-D-mannose) are shown in Fig. 1 for the dominant (in the case of these sugars) $^4C_1$ ring shape. The equatorial OH at C2 refers to D-glucose, while the axial OH indicates D-mannose, and the axial and equatorial dispositions the OH group at C1 define whether the molecule is the α- or β-compound, respectively. It is not necessary to study the energetics of both the D- and L-enantiomers because a $^1C_4$ L-sugar is the mirror image of the $^4C_1$ D-sugar.

The anomeric effect that was originally discovered for sugars [3–5] in aldo-pyrano-hexoses manifests itself as the substituent effect of electronegative groups at C1, which increases the population of the α anomer at the expense of the β form. For example, the proportion of the axial α-anomer is about 67% for D-mannose [3]. For other aldo-pyrano-hexoses, e.g. glucose, galactose, and gulose this effect is apparently weaker because the α anomers have populations of about 36, 31 and 18%, respectively [3].

Glucose has been the subject of extensive theoretical studies [6–10]. The HF/4-31G [9] and HF/6-31G(d) [10] calculations provide that the α-anomer

* Corresponding author.

PII S0166-1280(96)04545-9

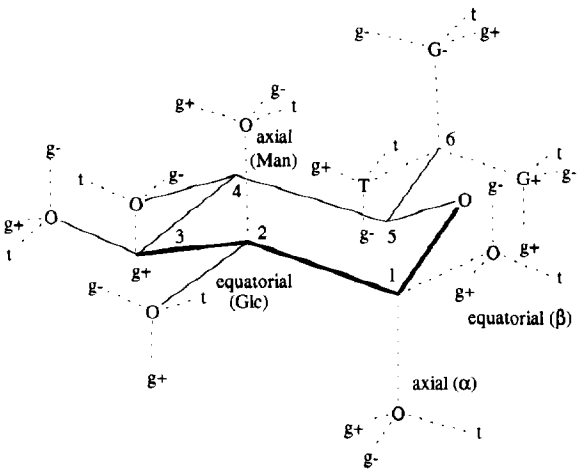

Fig. 1. Illustration of the conformational spaces of the $^4C_1$ pyranose rings of the (α,β)-D-glucose and mannose (OH axial at C2). The idealized C(x + 1)–Cx–O–H torsions are denoted by g$^+$, t and g$^-$ for gauche clockwise (60°), anti (180°), and gauche counterclockwise (− 60°) respectively where x = 1, 2, 3, 4. The T, G + and G − symbols denote the positions of the oxygen in the hydroxymethyl group (O5–C5–C6–O6 torsions). The idealized C5–C6–O6–H torsions are denoted by g + ,t and g − .

is the more stable by 2.2 and 1.2 kcal mol^{-1}, respectively. This varies from the experimental 0.3 kcal mol^{-1} preference for the β-form in aqueous solution. Lemieux et al. [11] showed, based on NMR data, that hydroxylic solvatation decreases the anomeric effect (i.e. it increases the preference of the β-anomer). The calculated results agree well with the experimental results in this respect for simple pyranoses [5,12,13] and their derivatives [14,15], although different conclusions have been drawn regarding the nature of the differential solvatation effect (i.e. whether it involves hydrogen bonding [11,13,16,17] or it is related mainly to electrostatic effects [12,14,18]). In addition to the solvent effects, the zero point energy difference between (ΔZPE) should also be considered [9]. This results in 0.5 kcal mol^{-1} preference of the β-anomer. The third source of the calculated α-anomer preference at HF/6-31G(d) level of theory is a basis set error of 0.5 kcal mol^{-1} [10]. The addition of a solvent effect of 0.5 kcal mol^{-1} to the basis set error and the ΔZPE would result in agreement with the observed (0.3 kcal mol^{-1}) preference for the β form.

The internal rotation of the hydroxymethyl group was also studied in a number of publications. Polavarapu and Ewig [9] proved that the conformation of the CH_2OH has no influence on the energy difference between the two anomers, at the HF/4-31G level of theory. Schleyer et al. [10] showed that this remains true at HF/6-31G(d) level of theory. NMR results for the CH_2OH group suggest that the G − and G + (see Fig. 1, the methoxy oxygens are denoted by capital G and T) conformations are populated in about 55:45 ratio at room temperature, while the population of the T conformation were considered negligible (less than 2%) [19]. At HF/4-31G level of theory the T conformation is the most stable [9]. However, the comparison of the Gibbs energies, instead of the electronic energies, shows that the G − conformer is slightly more stable, by 0.02 kcal mol^{-1} [8]. In the crystal structure of the α-D-glucose [20]. the latter, the G − orientation was found for the CH_2OH group. However, the crystal structure represents a conformer of considerably higher energy, by 8 kcal mol^{-1} at HF/6-31G(d) level of theory, because at this geometry the unfavourable orientations of the OH groups decreases the number of intramolecular hydrogen bridges [10].

In the present paper the conformational space of aldo-pyrano-hexoses is searched by the MM2*–SUMM method. During conformational searches pyranose rings were temporarily cleaved; thus, all twisted and boat ring conformations were screened as potential minima. We analyze the first 19 low energy structures at the HF3-21G, 6-31G and generalized gradient approximation (GGA) DFT levels of theory. The interactions of the hydroxyl groups are analyzed by the help of gradient vector field theory.

2. Computational methods

The search for stable conformers in the conformational space of aldo-pyrano-hexoses was carried out using the MACROMODEL 4.0 program package [21]. The MM2* force field available in MACROMODEL has been used which differs from the original MM2 force field [22] only in that it employs the point-charge Coulomb potential to describe the electronic–electrostatic interactions. The conformational space was searched using a particularly efficient SUMM (systematic unbounded multiple minimum) search technique [23] that is available in MACROMODEL. During conformational searches, aldo-pyrano-hexoses

were temporarily cleaved, according to the "ring-master" approach of Still and Galynker [24]. The 3500 structures generated by the SUMM procedure were re-closed and minimized to yield unique conformers within an energy window of 40 kJ mol^{-1} above the global minimum. Geometry optimizations were carried out with a truncated Newton conjugate gradient (TNCG) technique [25] with maximal number of iterations set to 150, and using a convergence criteria of 0.01 for gradient norm. This procedure resulted in 320 minima.

The first 19 minima obtained by the MM2*–SUMM search were further optimized by HF and generalized gradient approximation density functional (GGA–DFT) methods. The use of density functional methods might be advantageous to recover electron correlation effects that are not included in the HF method. Kohn and Sham [26] proved that the exact ground-state density and energy of a many-electron system may be found like that of a Hartree–Fock (HF) self consistent field (SCF) method. In the Kohn–Sham (KS) method, the HF exchange energy is replaced by the exchange-correlation energy that is a functional of the electron density and the HF exchange potential is replaced by the exchange-correlation potential, termed KS potential, which is the functional derivative of the exchange-correlation energy [27,28]. This formalism seems to be an economic alternative compared to the extremely expensive configuration-interaction-based methods used currently for the electron correlation. However, the exact molecular KS potentials are generally not known, consequently approximate potentials are used in the practical calculations. We employed the following combinations of the GGA–DFT functionals:

(i) BP or Becke–Perdew method, in which Becke's exchange functional [29] is combined with Perdew's correlation functional [30].

(ii) B3P is a hybrid method. It is a linear combination of various exchange and correlational functionals in the form:

$$A\cdot E_x[HF]+(1-A)\cdot E_x[S]+B\cdot\Delta E_x[B]+E_c[VWN]+C\cdot\Delta E_c[P86],$$

where E_x[HF], E_x[S] and ΔE_x[B] are the HF, Slater and Becke exchange functionals; and E_c[MN] and ΔE_c[P86] are the Vosko, Wilk and Nussair [31] and Perdew [30] correlation functionals, respectively. Note that ΔE_x[B] is a gradient correction to the S + WVN or LSDA, for exchange and ΔE_c[P86] is a gradient correction for correlation. The constants A, B and C are those determined by Becke by fitting heats of formations (A = 0.2, B = 0.72, C = 0.81) [32]. Note that Becke used the Perdew–Wang (PW91) functional instead of P86 [32].

(iii) B3LYP is a hybrid method. This functional was not published before the implementation into the GAUSSIAN 92/DFT [33]. It is a logical extension of Becke's three-parameter concept using different correlational functionals (e.g. LYP) in the form:

$$A\cdot E_x[HF]+(1-A)\cdot E_x[S]+B\cdot E_x[B]+(1-C)\cdot E_c[VWN]+C\cdot E_c[P86],$$

The constants A, B and C are selected to be equal to those determined by Becke for the B3P method [32].

GAUSSIAN 92/DFT [33] uses numerical quadrature to evaluate the DFT integrals. The quadrature scheme is defined by the number of points in the radial and angular directions. The geometries were optimized with a normal grid (50 radial shells, 194 angular points per shell, pruned to about 3000 points per atom).

The HF and GGA–DFT calculations were carried out using 3-21G [34] and 6-31G(d) [35] basis sets.

The properties of the gradient vector field of the electron density, $\nabla\rho(\mathbf{r})$, were calculated from the wave functions calculated by the G92/DFT using AIMPAC package, [36] which was modified in our laboratory to perform the grid calculations. The gradient vector field theory for the analysis of electron density has been pioneered by Bader and it has been reviewed recently [37,38]. Using this approach, gradient trajectories of the electron density can be identified. The gradient vector field of the electron density, $\nabla\rho(\mathbf{r})$, has a set of attractors, where the basin of an attractor is defined by the "catchment region" of points for which this attractor is the so-called ω-limit. These basins are recognized as atoms in molecules and an atom in a molecule is defined as a set of points in three-dimensional space bounded by a zero-flux surface. Two interacting atoms are connected by a maximum electron density (MED) path which terminate near the neighbouring nuclei (attractors). The MED path is alternatively called

Table 1
MM2, HF/3-21G, HF, BP, B3P and B3LYP/6-31G(d) energies (E) and energy differences (ΔE) of the first 19 low energy conformations and configurations of pyranose rings provided by the MM2–SUMM search[a]

Torsional angles							MM2		HF/3-21G		HF/6-31G(d)		BP/6-31(d)		BP/6-31(d)	B3LYP/6-31G(d)	
No.	1	2	3	4	5	6	E^b	ΔE^c	E^d	ΔE^c	E^d	ΔE^c	E^d	ΔE^c	E^d	ΔE^c	E^d
1	g −	g + (a)	g +	g −	**T**	t	− 113.67	− 1.43	− 679.56049	1.35	− 683.33233	1.08	− 687.15585	1.29	− 688.88289	1.12	
2	t	t(a)	g −	**t**	T	g +	− 112.46	− 1.14	− 679.56006	1.62	− 683.33227	1.12					
3	g −	g + (a)	g +	g −	G −	g +	− 111.50	− 0.91	− 679.55737	3.31	− 683.33266	0.87					
4	t	t(a)	g −	**t**	G +	g −	− 111.50	− 0.91	− 679.55582	4.28							
5	t(a)	g + (a)	g +	g −	T	t	− 109.59	− 0.45	− 679.56379	− 0.71	− 683.33292	0.71	− 687.15468	2.02	− 688.88197	1.74	
6	t(a)	g + (a)	g +	g −	G −	g +	− 108.04	− 0.08	− 679.56119	0.91	− 683.33366	0.24	− 687.15632	0.99			
7	**t(a)**	**g +**	**t**	**t**	**T**	**g +**	**− 107.70**	**0.00**	**− 679.56265**	**0.00**	**− 683.33405[e]**	**0.00**	**− 687.15790**	**0.00**	**− 688.88469**	**0.00**	**− 687.15331**
8	g −	g + (a)	g +	g −	T	g −	− 107.20	0.12	− 679.55928	2.11							
9	**t(a)**	**g +**	**t**	**t**	**G +**	**g −**	**− 107.02**	**0.16**	**− 679.55931**	**2.09**	**− 683.33370**	**0.22**	**− 687.15644**	**0.92**	**− 688.88321**	**0.93**	
10	g −	g + (a)	g +	g −	G −	t	− 106.34	0.33									
11	t	t	t(a)	g − (a)	G −	g +	− 105.97	0.41	− 679.56537	− 1.71	− 683.33400	0.03			− 688.88503	− 0.20	
12	**t**	**t**	**t**	**t**	**T**	**g +**	**− 105.77**	**0.46**	**− 679.55582**	**4.28**	**− 683.33219[e]**	**1.17**	**− 687.15442**	**2.18**	**− 688.88162**	**1.93**	**− 687.15031**
13	**t(a)**	**g +**	**t**	**t**	**G −**	**g +**	**− 105.44**	**0.54**			**− 683.33386**	**0.12**			**− 688.88367**	**0.64**	
14	**t**	**t**	**t**	**t**	**G +**	**g −**	**− 105.33**	**0.57**	**− 679.55250**	**6.37**	**− 683.33194**	**1.32**	**− 687.15320**	**2.95**	**− 688.88034**	**2.72**	**− 687.14918**
15	t	t(a)	g −	**t**	G −	t	− 105.13	0.61	− 679.55031	7.74							
16	t(a)	g + (a)	g +	g −	G +	g −	− 104.43	0.78	− 679.5561	4.11	− 683.33057	2.18					
17	t	t(a)	g −	t	G +	g +	− 103.76	0.94	− 679.55002	7.93	− 683.32759	4.06					
18	**t**	**t**	**t**	**t**	**G −**	**g +**	**− 103.61**	**0.98**	**− 679.55469**	**5.00**	**− 683.33227**	**1.11**			**− 688.88079**	**2.45**	
19	t(a)	g + (a)	g +	g −	T	g −	− 103.51	1.00	− 679.56265	− 0.01	− 683.33278	0.80					

[a] The six torsional angles are denoted as in Fig. 1. The axial positions of the hydroxyl groups denoted by (a), e.g. for the first position (a) denotes the α anomer, for the second position it denotes mannose. Gulose has two axial hydroxyls in the positions 3 and 4. The glucose rotamers are in bold.

[b] KJ mol^{-1}.

[c] kcal mol^{-1}.

[d] Hartrees.

[e] In agreement with Ref. [10].

bond path. The necessary condition for a bond is the existence of a bond path between the two nuclei. The molecular graph is the network of bond paths. Along a bond path there exists a critical point where the $\nabla\rho(\mathbf{r}) = 0$. This critical point is called bond critical point (BCP) and it is a minimum of $\rho(\mathbf{r})$ along the MED path and a maximum of $\rho(\mathbf{r})$ in all directions perpendicular to the MED path. It corresponds to a multiple saddle point of $\rho(\mathbf{r})$ in three dimensions. This saddle point may be characterized by the three eigenvalues of the second derivative (Hessian) matrix, the first two eigenvalues (λ_1 and λ_2) are negative, the third eigenvalue (λ_3) is positive at BCP. In a usual sigma bond the two negative eigenvalues are equal to each other because of the cylindrical symmetry. In the double bonds and ring bonds the negative eigenvalues are different ($\lambda_1 < \lambda_2$) the bond is elliptic. The ellipticity is defined as: $\varepsilon = \lambda_1/\lambda_2 - 1$. Inside of a ring of the MED paths there exists a ring critical point (RCP). In this type of saddle point the first eigenvalue is negative, and the two other eigenvalues are positive. This means that the electron density is minimum in two directions (in a plane) in this point. For the symmetric rings, the two positive eigenvalues are equal to each other. During the formation of a ring, a conflict point appears first because one BCP and RCP merge, resulting in an elliptic critical point with an eigenvalue of nearly zero.

The trace of the Hessian matrix, the Laplacian of the electron density $\rho(\mathbf{r})$, $\nabla^2\rho(\mathbf{r})$, is of fundamental physical significance. The detailed analysis shows that the sign of $\nabla^2\rho(\mathbf{r})$ is determined by the relative magnitudes of the local values of the potential and kinetic energy densities. In regions where $\nabla^2\rho(\mathbf{r})$ is negative, the potential energy is dominant and the negative charge is concentrated. In the regions with positive $\nabla^2\rho(\mathbf{r})$ the kinetic energy density dominates and a depletion of negative charge occurs.

The visualization of the results was created by our programs written with the Explorer™ development package. All calculations were performed on Silicon Graphics workstations.

3. Results and discussion

The MM2*–SUMM results, summarized for the first 19 minima in Table 1, show that the first six lowest energy conformers are various $^4C_1$ D-mannose conformations (axial OH at the C2 in Table 1). The various C_1, aldo-pyrano-hexose conformations and configurations are numbered according to the MM2* energy sequence and the conformations and configurations are notated according to Fig. 1. The MM2* results contradict experimental results providing that the anomer of the mannose is more stable than the β-anomer. Further mannose conformations can he found in the rows 8, 10, 15, 16, 17 and 19 of Table 1. The remaining conformations and configurations, shown in Table 1, are various glucose conformations,

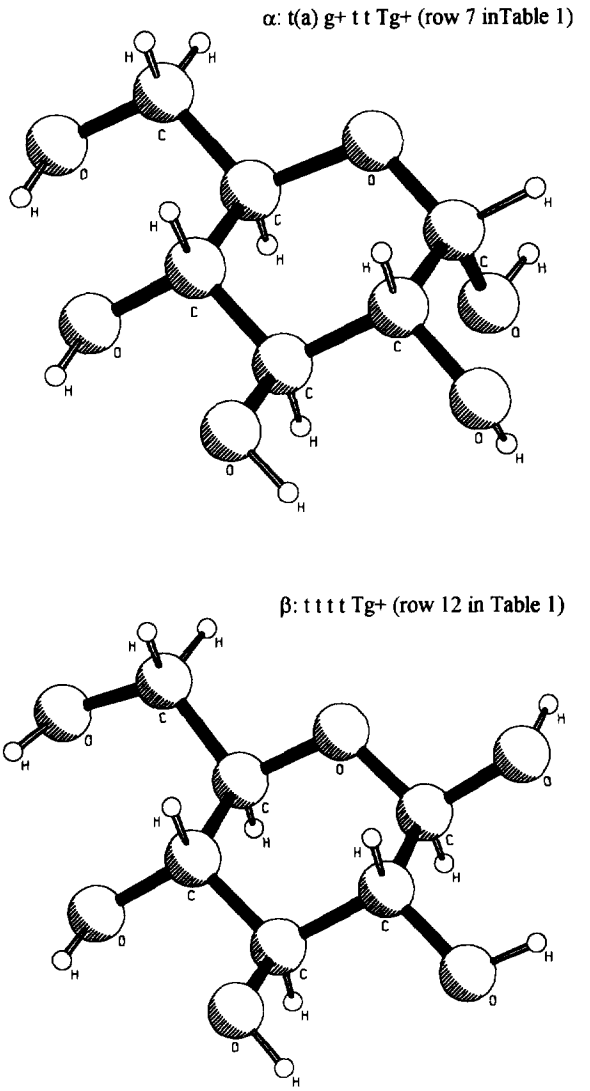

Fig. 2. The α and β anomers $^4D_1$-glucose.

the only exception is a gulose (row 11). The results show qualitatively that the three-fold rotator model is not suitable for the description of the rotation of the OH groups of the aldo-pyrano-hexoses. The relative orientations of the four OH groups on the C1–C4 atoms of the pyranose ring allows for strong coupling. In the most stable conformation, the number of possible OH···O interactions is maximal and this leads to the formation of an intramolecular chain of OH groups. The formation of these bridges distort the ideal three-fold potential energy surface and counterclockwise, t t t t Tg + like (e.g. conformations 2, 4, 7, 9, 12, 13, 14, and 18 in Table 1) or clockwise, g − g + (a) g + g − Tt like (e.g. conformations 1, 3, 5, 6, 8, etc. in Table 1), patterns appear (the order of the letters follows the clockwise sequential numbers of the carbon atoms). These effects dramatically reduce the number of possible rotamers. Fig. 2 shows the lowest energy α- and β-D-glucose conformations with counterclockwise OH orientations (conformations 7 and 12 in Table 1).

The orientation of the CH_2OH group is influenced only slightly by the formation of the intramolecular OH chains. The CH_2OH group shows the expected three-fold rotation pattern (c.f. rows 5, 6, 16 or 2, 4, 15 or 7, 9, 13 (triplets) in Table 1).

The HF/3-21G and 6-31G(d) results in Table 1 show clearly that the MM2* energy order does not agree with the HF energy order and even at the HF level the basis set dependence of the energy differences is large. To facilitate the comparisons, the relative energies compared to the lowest energy α-D-glucose (7th row in Table 1) are shown in separate columns of Table 1. The HF/3-21G method provides that one of the mannose and gulose conformations (5th and 11th row in Table 1) have an energy that is lower than the reference (7th row in Table 1). The HF/6-31(d) energy order differs from that obtained at the HF/3-21G level (e.g. the structure 11 is less stable than the structure 7) and the former method results in smaller energy differences. Fig. 3 shows the energy differences in graphical form to facilitate the

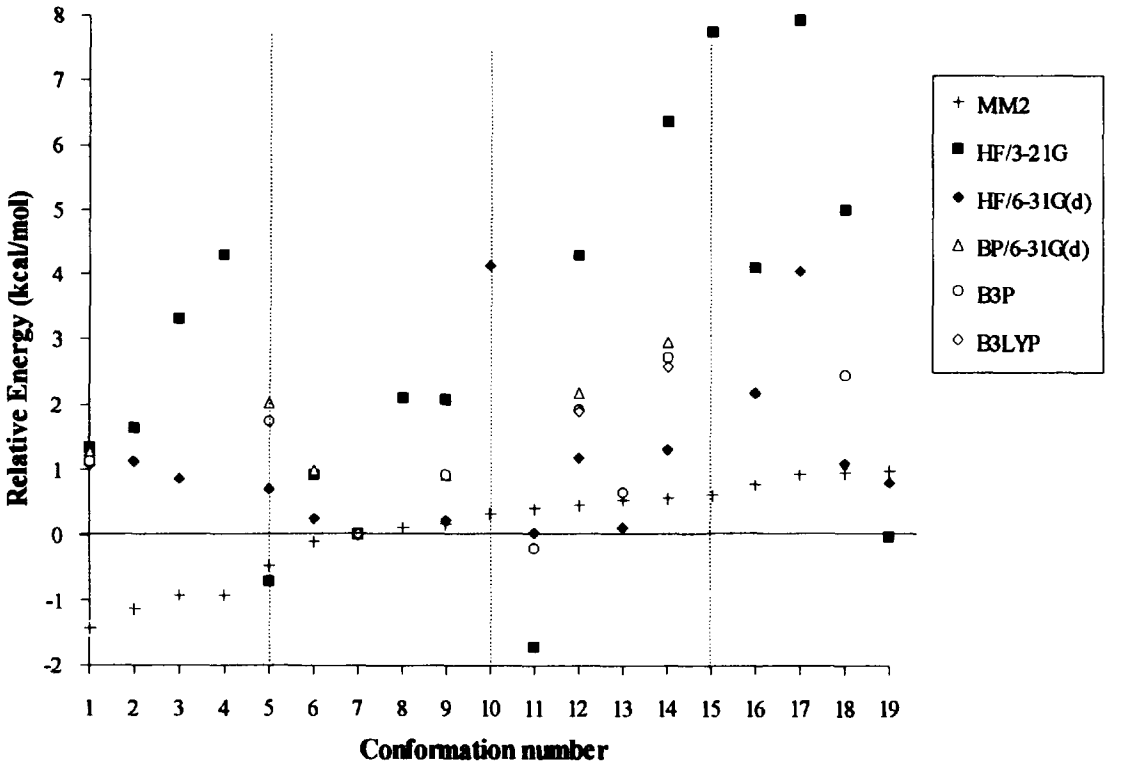

Fig. 3. The relative energy differences of aldo-pyrano-hexoses calculated with MM2, HF/3-21G, HF, BP, B3P and B3LYP/6-31G(d) methods. The numbering of conformations is given in Table 1.

comparison. The HF results are in agreement with experiment suggesting that the α-anomers of the $^4C_1$ D-mannose (rows 5 and 6 in Table 1) are more stable than the corresponding β-anomers (rows 1 and 3 in Table 1). The energy difference is about 2 and 0.4 kcal mol^{-1} at HF/3-21G and HF/6-31G(d) levels of theory, respectively.

Our recent GGA–DFT results [39] for 1,2-ethanediol show that the theoretical predictions are consistent with the experimental observations. There exist two conformers (gGg − and tGg −) which are nearly equally stable. In this respect the GGA–DFT results, especially the B3P/6-311G(d,p) results, are in good agreement with the MP2/6-311G(d,p), and MP2/cc-pVDZ results. The B3P/6-31G(d) results are close to the CCSD(T)/cc-pVDZ//MP2/cc-pVDZ and MP4/6-311G(d,p)//MP2/6-311G(d,p) results. The HF/3-21G method provides an exaggerated stability for the tGg-conformation compared to the tGt and tGg rotamers.

For aldo-pyrano-hexoses, the GGA–DFT methods follow approximately the HF/6-31G(d) ordering; however, they result in considerably larger energy differences. It is seen that the GGA–DFT methods agree well with each other and they may differ considerably (by 2–3 kcal mol^{-1}) from HF3-21G results (Fig. 3). The α-anomer of the $^4C_1$ D-glucose is predicted to be more stable than the β-anomer by 1.8–2.2 kcal mol^{-1} depending on the GGA–DFT functional (c.f. rows 7 and 12 in Table 1). The GGA–DFT results are in disagreement with experiment suggesting that the α-anomer of the $^4C_1$ D-mannose is less stable than the corresponding β-anomer (c.f. rows 5 and 1 in Table 1).

Next we compared the total energy of the t(a) t t t Tg + rotamer (not shown in Table 1) of α-D-glucose to that of the lowest energy rotamer (t(a) g + t t Tg + in row 7 in Table 1) at HF, BP and B3P/6-31G(d) levels of theory. In the former conformation, the interaction between the first two OH groups is broken, while the interaction between the other OH groups is conserved. The breaking of the OH···O chain between the C1 and C2 atoms results in a higher energy, by 3.70, 5.06 and 5.02 kcal mol^{-1} respectively.

Table 2 shows the geometrical parameters for some selected conformations at HF/3-21G level of theory. The comparison of the C1–O5, C1–O1 and C1–H distances of the conformers 7 and 12 reveal that the geometric consequences of the anomeric effect are reproduced at HF/3-21G level of theory. The C5–O–C1 and O–C1–1 bond angles are smaller in β-anomers. The dihedral angles frequently show large deviation, in some cases as large as 20°, from the ideal angles, because of the OH···O interactions.

Table 3 shows the GGA–DFT geometrical parameters for six low energy rotamers of α and β-D-glucose. The longest bond lengths are provided by the BP method. The HF exchange included in the B3P method provide slightly shorter C–O bonds. In the α-anomer the C1–O5 bond length is 0.01 Å shorter than the C1–O1 bond length. In the α-anomer the C1–O5 bond length is 0.03 Å longer than the C1–O1 bond length. The C1–H bond length is 0.01 Å longer in β-anomer than in α-anomer. The C5–O–C1 and O–C1–O bond angles are 2.5 and 4° smaller in β-anomer than in α-anomer respectively. The differences mentioned are seemingly

Table 2
Geometrical parameters for selected conformations at HF/3-21G level of theory[a]

	Bond lengths				Bond angles			Dihedral angles					
No.	C5–O5	C1–O5	C1–O1	C1–H	C5–O–C1	O–C1–O	C1–O–H	1	2	3	4	5	6
2	1.447	1.423	1.416	1.083	115.5	107.0	110.1	159.2	201.9	− 82.7	161.3	172.0	46.9
3	1.445	1.436	1.396	1.079	116.4	108.8		− 44.9	47.7	50.5	− 84.3	− 61.5	57.1
4	1.457	1.422	1.416	1.087	115.6	107.4	110.6	197.6	200.9	− 81.9	167.6	58.7	− 54.3
5	1.444	1.422	1.422	1.077	116.4	110.4	111.1	180.1	46.2	49.3	− 45.4	186.8	179.4
6	1.453	1.423	1.421	1.077	115.7	110.4	111.3	181.0	47.5	51.8	− 85.9	− 62.2	54.8
7	1.451	1.415	1.428	1.078	116.3	112.2	112.2	181.2	80.0	189.8	167.3	171.6	44.6
9	1.461	1.415	1.427	1.078	116.5	112.3	112.3	180.6	79.2	189.4	168.7	57.6	− 54.8
12	1.448	1.426	1.408	1.085	114.3	109.6	111.2	191.7	178.1	187.6	168.9	171.6	44.5

[a] Bond lengths are in Å, the angles are in degrees.

Table 3
Geometrical parameters of selected $^4C_1$ D-glucose conformations calculated by HF and GGA–DFT methods using 6-31G(d) basis set[a]

No.	Conformation	Method	Bond lengths				Bond angles			Dihedral angles					
			C5–O5	C1–O5	C1–O1	C1–H	C5–O–C1	O–C1–H	C1–O–H	1	2	3	4	5	6
7	t(a) g + t t Tg +	Hf[b]	1.417	1.386	1.394	1.082	116.9	112.3	109.8	184.5	79.5	185.7	172.5	166.4	53.4
7	t(a) g + t t Tg +	BP	1.452	1.419	1.429	1.107	115.0	113.5	107.4	188.9	80.4	189.0	172.2	169.7	50.5
7	t(a) g + t t Tg +	B3P	1.431	1.400	1.411	1.097	115.4	113.2	108.2	187.7	80.5	188.5	170.7	169.3	50.5
7	t(a) g + t t Tg +	B3LYP	1.441	1.408	1.419	1.097	115.7	113.1	108.1	186.6	80.4	188.0	171.5	168.1	50.7
9	t(a) g + t t G + g −	BP	1.461	1.420	1.429	1.107	115.1	113.5	107.7	189.6	79.4	187.7	165.6	58.4	− 52.1
9	t(a) g + t t G + g −	B3P	1.439	1.402	1.410	1.097	115.5	113.2	108.5	188.0	79.4	187.7	166.8	58.0	− 53.2
12	tttt Tg +	BP	1.442	1.435	1.404	1.118	112.2	108.9	107.4	175.0	178.9	184.6	173.5	169.6	50.7
12	ttttTg +	B3P	1.423	1.414	1.388	1.107	112.7	109.2	108.2	176.6	178.8	184.6	172.4	169.1	50.6
12	ttttTg +	B3LYP	1.432	1.421	1.396	1.106	113.1	109.0	108.1	177.8	179.5	184.1	173.0	168.6	51.1
13	t(a) g + t t G − g +	B3P	1.438	1.403	1.410	1.097	116.2	112.8	108.4	189.0	78.4	189.1	171.4	− 56.6	52.6
14	t t t t G + g −	BP	1.449	1.438	1.403	1.116	112.3	109.1	107.6	172.8	179.9	183.6	168.3	58.5	− 51.8
14	t t t t G + g −	B3P	1.430	1.417	1.388	1.106	112.9	109.4	108.4	173.0	179.6	183.9	169.0	57.9	− 52.3
18	t t t t G − g +	B3P	1.429	1.414	1.388	1.106	113.6	109.1	108.3	173.8	178.7	184.0	172.4	− 56.3	51.2

[a] Bond lengths are in Å, the angles are in degrees.
[b] Some bond lengths and angles are also given in Ref. [10].

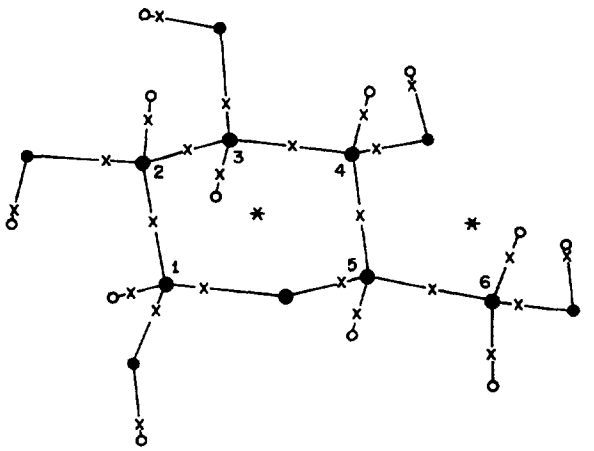

Fig. 4. Illustration of the results of the gradient vector field analysis for t(a) g + t t T g + rotamer of (α-D-glucose calculated at HF/6-31G(d) level of theory. Ring critical points are marked by *, bond critical points are marked by ×.

method-independent. Comparison of the C1–O–H bond angles in Table 2 and Table 3 provide that the HF/3-21G method gives a too large bond angle. The wide C–O–H bond angle is clearly the result of the basis set deficiency of the 3-21G basis set. A polarization function on the O atom would result in better bond angles (c.f. HF/6-31G(d) results in Table 3).

The method dependence of the six dihedral angles in Table 3 is small, which is rather encouraging. However, the differences between the HF and DFT dihedral angles in Table 3 show that correlation effects may play an important role in determining, the orientation of the OH hydrogens.

Next we performed a gradient vector field analysis of the electron density of the t(a) g + t t Tg + rotamer of C_1 (α-D-glucose at HF and BP/6-31G(d) levels of theory. The two results differ marginally from each other. The HF results are presented in Fig. 4. The OH bond critical points (BCP) are shifted toward the hydrogen atoms and the C–O BCPs are closer to C atoms, as expected. The ring critical point (*) in the middle of the pyranose ring is well visible. There is a surprising ring critical point between the hydroxymethyl group and the fourth hydroxyl group. It is interesting, because there is no closed ring around it. This feature will be discussed later. The algorithms of the AIMPAC program, used in this paper for the critical point search, did not find any critical points between the hydroxyl groups. This means that there is no hydrogen bond in this sense between the hydroxyl groups. A more detailed investigation resulted that the critical point of the electron density between the hydroxyl groups of the tGg − conformer of the 1,2-ethanediol appears as a weak minimum in a slightly varying low density (0.012–0.017 au) electron gas [40]. The critical point is characterized by a small positive Laplacian (0.053–0.064 au) and large (2.2) ellipticity, possibly caused by the merging of a BCP with a ring critical point. The 3D analysis shows that at small values of $|\nabla\rho|$ an elliptic lens-shaped surface appears around this critical point.

The positions, the electron densities and Laplacians of some selected critical points are summarized in Table 4. The C5–O5 bond shows the characteristics of a normal sigma C–O bond. The bond critical point is close to the carbon atom and the value of the Laplacian is only slightly negative. The ellipticity of

Table 4
Results of the gradient vector field analysis of HF/6-31G(d) electron density for α-D-glucose[a]

A	B	r(A − B)	r_c(A)	r_c(B)	ρ_c	$\nabla^2\rho_c$	ε_c	λ_1	λ_2	λ_3
BCP										
C5	O5	1.417	0.449	0.969	0.248	− 0.046	0.014	− 0.447	− 0.441	0.842
C1	O5	1.386	0.442	0.945	0.277	− 0.223	0.202	− 0.640	− 0.532	0.949
C1	O1	1.394	0.442	0.952	0.269	− 0.158	0.198	− 0.606	− 0.505	0.953
C1	C2	1.526	0.782	0.744	0.276	− 0.808	0.069	− 0.588	− 0.550	0.330
C1	H	1.082	0.698	0.385	0.302	− 1.187	0.031	− 0.860	− 0.834	0.506
O1	H	0.949	0.767	0.182	0.364	− 2.099	0.019	− 1.891	− 1.856	1.648
RCP										
OH (4)	06		1.139	1.432	0.011	0.065		− 0.008	0.025	0.048
O5	C4		1.390	1.426	0.019	0.133		− 0.016	0.071	0.079

[a] r_c(A) and r_c(B) are the distances (A) from the atom A and B to the bond critical point respectively. ρ_c is the electron density (e/au^3), $\nabla^2\rho_c$ is the Laplacian of ρ_c, ε_c is the ellipticity of ρ_c and λ − s are the curvatures of the ρ_c at the bond or ring critical points (BCP or RCP respectively).

the bond is negligible. However, in the C1–O5 and C1–O1 bonds the electron density in the BCP is larger, the Laplacian is more negative and a considerable ellipticity appears. This is a clear sign of electron delocalization and this delocalization is responsible for the anomeric effect. The ring critical point between the hydroxymethyl group and the fourth hydroxyl group is characterized by a small positive Laplacian (0.065 au) and large (3.0) ellipticity. This critical point appears to be a conflict point in which a RCP and a BCP are shifted together. Similar BCP–RCP merging was found by Cioslowsky for H–H interactions [41]. This weak interaction is essentially similar to the weak interaction found between the hydroxyl groups of the 1,2-ethanediol [40]. However, the spatial arrangment of the interaction is somewhat different (6 membered ring vs. 5 membered ring).

In order to visualize the problem, we present the relief map for the absolute values of the electron density gradients, $|\nabla\rho|$, in Fig. 5. The two RCPs may be well identified and the asymmetric nature of the conflict point is well visible from Fig. 5. Fig. 5 shows again that there are no BCPs between the other OH groups.

4. Conclusions

The following conclusions can be drawn from the discussion above:

1. The MM2* method does not provide an energetic

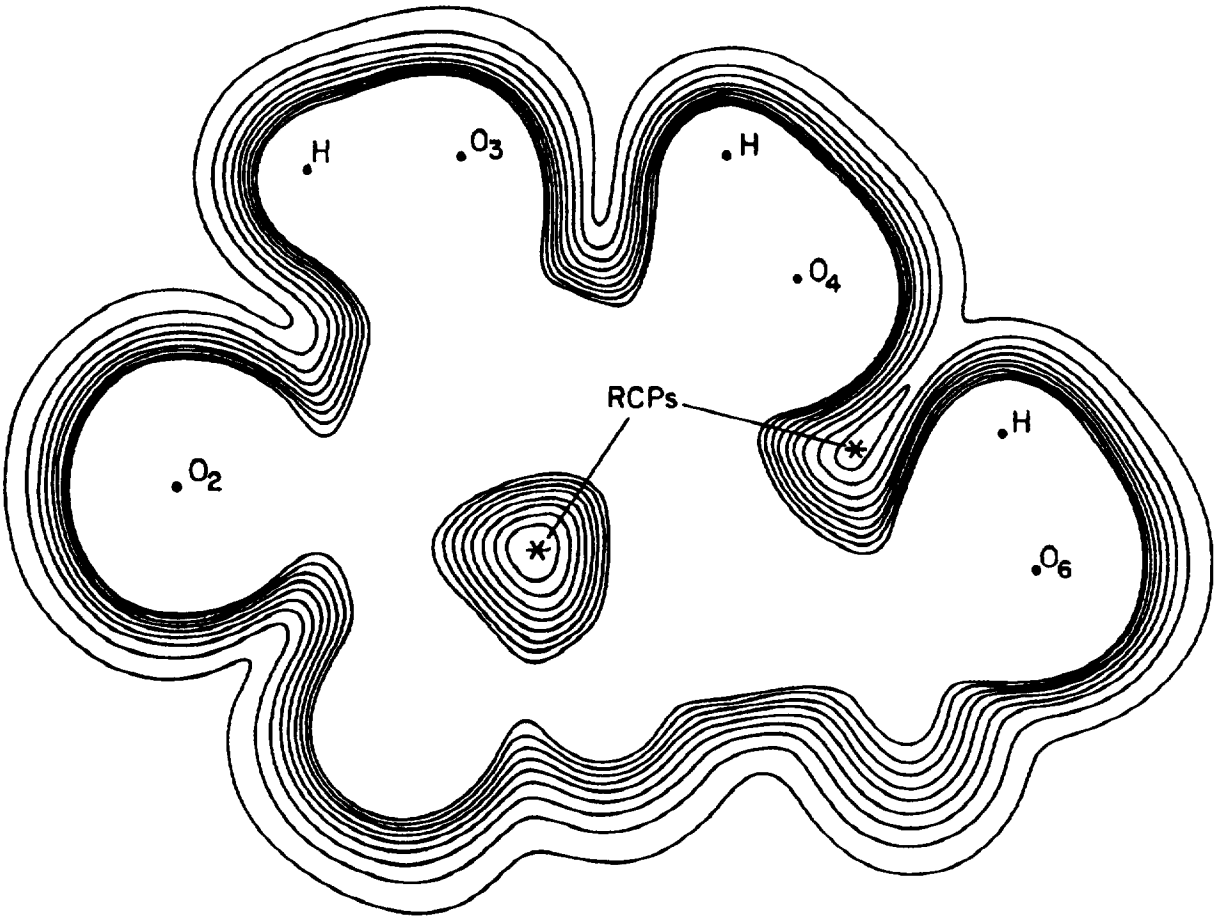

Fig. 5. Relief map of the absolute value of the HF/6-31 G(d) electron density gradient, $|\nabla\rho|$, for t(a) g + t t Tg + rotamer of $^4C_1$ (α-D-glucose in the plane containing the O4, H6 and the two ring critical points. The innermost contour corresponds to a gradient value of 0.01 au and the outermost contour has a value of 0.001 au.

order for the various rotamers and conformers of the pyranose rings, which is in agreement with the HF results. Serious differences appear in Table 1 and Fig. 3. The MM2* method appears to reverse erroneously the experimental preference between the α and β anomers of $^4C_1$ D-mannose.

2. The HF/3-21G method provides large energy differences. The HF/6-31G(d) method provides considerably smaller energy differences and somewhat different energy ordering for the conformers investigated in the present paper. The HF/3-21G method reproduces correctly the experimental results that the α-anomer of $^4C_1$ D-mannose is the more stable.
3. The deficiencies of the HF/3-21G method result in the wrong C–O–H equilibrium bond angles and C–C–O–H dihedrals.
4. The GGA–DFT methods provide somewhat larger energy differences than the HF6-31G(d) method and they reflect correctly the expected structural changes due to the inclusion of the electron correlation relative to the HF method. The BP, B3P and B3LYP methods provided consistent results.
5. The MM2*, HF and GGA–DFT results are in agreement with each other in that the orientation of the four OH groups on the C1–C4 atoms of the pyranose ring show strong coupling. The most stable conformations tend to maximize the number of possible OH···O interactions and thus provide an intramolecular chain of OH groups. The formation of these bridges distorts the ideal three-fold potential energy surface and counterclockwise, t t t t Tg + like or clockwise, g − g + (a) g + g − Tt like patterns appear. These effects greatly reduce the number of possible rotamers.
6. The AIMPAC results of the HF/6-31G(d) electron density analysis suggest that the OH···O interactions are not a well-defined hydrogen bond, because there exists no BCP between the hydrogen and oxygen atoms of the neighbouring OH groups. Only a distorted conflict point has been found between the O4–H and the CH_2OH group.
7. There is a large ellipticity at bond critical points of the C1–O bonds. This is a clear sign of electron delocalization. The values of the Laplacians of the two C1–O bonds are relatively large and negative. The electron densities at the C1–O bond critical points are also larger than at the other C–O BCPs.

Acknowledgements

The financial support of the Hungarian Research Foundation (OTKA T14975, and T16328) is acknowledged. The continued financial support of the Natural Sciences and Engineering Research Council (NSERC) is gratefully acknowledged.

References

[1] R.E. Reeves, J. Am. Chem. Soc., 71 (1949) 215.
[2] M.K. Dowd, A.D. French and P.J. Reilly, Carbohydr. Res., 2264 (1994) 1.
[3] (a) S.J. Angyal, Adv. Carbohydr. Chem. Biochem., 42 (1984) 15, (b) S.J. Anoyal, Adv. Carbohydr. Chein. Biochem., 49 (1991) 19.
[4] A.J. Kirby, The Anomeric Effect and Related Stereoelectronic Effects at Oxygen, Springer, New York, 1983.
[5] I. Tvaroska and T. Bleha, Adv. Carbohydr. Chem. Biochem., 47 (1989) 45.
[6] J.W. Brady, J. Am. Chem. Soc., 111 (1989) 5155.
[7] B.P. Van Eijck, L.M.J. Kroon-Batenburg and J.J. Kroon, Mol. Struct., 237 (1990) 315.
[8] S. Ha, J. Gao, B. Tidor, J.W. Brady and M.J. Karplus, Am. Chem. Soc., 113 (1991) 553.
[9] P.L. Polavarapu and C.S. Ewig, J. Comput. Chem., 13 (1992) 1255.
[10] U. Salzner and P.v.R. Schleyer, J. Org. Chem., 59 (1994) 2138.
[11] R.U. Lemieux, Explorations with Sugars: How Sweet it Was, American Chemical Society, Washington, DC, 1990, and references cited therein.
[12] I. Tvaroska and T. Kozár, Theor. Chim. Acta, 70 (1986) 99.
[13] F. Franks, Pure Appl. Chem., 59 (1987) 1189.
[14] I. Tvaroska and T. Kozár, Int. J. Quantum Chem., 23 (1983) 765.
[15] C.J. Cramer, J. Org. Chem., 57 (1992) 7034.
[16] M.J. Tait, A. Suggett, F. Franks, S. Ablett and P.A. Quickenden, J. Solution Chem., 1 (1972) 131.
[17] A. Suggett, J. Solution Chem., 5 (1976) 33.
[18] W.L. Jorgensen, J. Am. Chem. Soc., 103 (1981) 335.
[19] Y. Nishida, H. Ohrui and H. Meguro, Tetrahedron Lett., 25 (1984) 1575.
[20] G.M. Brown and H.A. Levy, Acta Crystallogr., Sect. B, (1979) 656.
[21] W.C. Still, MACROMODEL 4.0, Columbia University, USA.
[22] N.L. Allinger, J. Am. Chem. Soc., 99 (1977) 8127.
[23] J.M. Goodman and W.C. Still, J. Comput. Chem., 12 (1991) 1110.
[24] W.C. Still and I. Galynker, Tetrahedron, 37 (1981) 3981.
[25] (a) J.W. Ponder and F.M. Richards, J. Comput. Chem., 8 (1987) 1016. (b) T. Schlick and M. Overton, J. Comput. Chem., 8 (1987) 1025.
[26] W. Kohn and L.J. Sham, Phys. Rev. A, 140 (1965) 1113.

[27] R.G. Parr and W. Yang, Density Functional Theory of Atoms and Molecules, Oxford University Press, New York, 1989.
[28] R.M. Dreizler and E.K.U. Gross, Density Functional Theory, Springer, Berlin, 1990.
[29] A.D. Becke, Phys. Rev. A, 1988, 38, 3098.
[30] J.P. Perdew, Phys. Rev. B, 33 (1986) 8822.
[31] S.H. Vosko, L. Wilk and M. Nussair, Can. J. Phys., 58 (1980) 1200.
[32] A.D. Becke, J. Chem. Phys., 98 (1993) 5648.
[33] M.J. Frisch, G.W. Trucks, M. Head-Gordon, P.M.W. Gill, M.W. Wong, J.B. Foresman, B.G. Johnson, H.B. Schlegel, M.A. Robb, E.S. Replogle, R. Gomperts, J.L. Andres, K. Raghavachari, J.S. Binkley, C. Gonzalez, R.L. Martin, D.J. Fox, D.J. DeFrees, J. Baker, J.J.P. Stewart and J.A. Pople, GAUSSIAN 92/DFT, Revision F, Gaussian, Inc., Pittsburgh PA, 1993.
[34] I.S. Binkley, I.A. Pople and W.J. Hehre, J. Am. Chem. Soc., 102 (1980).939.
[35] W.J. Hehre, R. Ditchfield and J.A. Pople, J. Chem. Phys. 56 (1972) 2257.
[36] R.F.W. Bader's laboratory, AIMPAC, McMaster University, Hamilton, ON, L8S 4M1, Canada.
[37] R.F.W. Bader, Chem. Rev., 91 (1991) 993.
[38] R.F.W. Bader, Atoms in Molecules—A Quantum Theory, Oxford University Press, 1990.
[39] G.I. Csonka and I.G. Csizmadia, Chem. Phys. Lett., 243 (1995) 419.
[40] G.I. Csonka, N. Anh, J. Ágnyán and I.G. Csizmadia, Chem. Phys. Lett., 245 (1995) 129.
[41] J. Cioslowsky and S.T. Mixton, Can. J. Chem., 70 (1992) 443.